Journal of Catalysis 259 (2008) 85–95

Contents lists available at ScienceDirect

Journal of Catalysis

www.elsevier.com/locate/jcat

Activated takovite catalysts for partial hydrogenation of ethyne, propyne, and propadiene

Sònia Abelló [a], Danny Verboekend [a], Blaise Bridier [a], Javier Pérez-Ramírez [a,b,*]

[a] Institute of Chemical Research of Catalonia (ICIQ), Avinguda Països Catalans 16, 43007 Tarragona, Spain
[b] Catalan Institution for Research and Advanced Studies (ICREA), Passeig Lluís Companys 23, 08010 Barcelona, Spain

ARTICLE INFO

Article history:
Received 6 May 2008
Revised 19 July 2008
Accepted 25 July 2008
Available online 28 August 2008

Keywords:
Selective hydrogenation
Alkyne
Diene
Alkene
Ni–Al oxides
Takovite
Hydrotalcite
Operando spectroscopy
Catalyst activation
Carbon deposits

ABSTRACT

The gas-phase hydrogenation of ethyne, propyne, and propadiene was investigated over partially reduced Ni–Al mixed oxides derived from takovite, a hydrotalcite-type compound. The unique attributes of the hydrotalcite route leads to more active and selective catalysts compared to conventional Ni/Al_2O_3 prepared by impregnation. Tuning calcination and reduction conditions of the catalyst precursor is essential to optimize the hydrogenation performance. The best catalyst, calcined and reduced at 773 K, rendered stable propene yields up to ca. 65% and consisted of a $Ni(Al)O_x$ solid solution with 55% of the total bulk nickel in reduced form and surface enrichment by aluminum. Sintering of NiO and crystallization of $NiAl_2O_4$ at high calcination temperature induce lower activity. The alkyne or diene conversion increases with the percentage of metallic Ni in the samples, while an optimal degree of nickel reduction maximizes the monoalkene selectivity. Below the optimum, oligomer formation is favored and above the optimum, alkane production increases. A similar pattern was found for the H_2/HC ratio. The alkene selectivity experiences a dramatic increase in early stages of the reaction, which correlated with the build-up of C-containing species on the catalyst (sub-)surface. These selectivity-enhancing species are formed at specific reaction temperatures, highlighting the relevance of the testing procedure on assessing hydrogenation catalysts. The catalytic performance is strongly influenced by the hydrocarbon substrate. In contrast to propyne and propadiene, ethyne hydrogenation led to a C_2H_4 yield of only 6%.

© 2008 Elsevier Inc. All rights reserved.

1. Introduction

An important segment of commercial catalytic hydrogenations in the petrochemical and fine (specialty) chemical industries is the selective transformation of organic compounds with conjugated or cumulative double bonds and/or triple bonds into the corresponding monoalkene [1–5]. Supported palladium (<0.1 wt% Pd on low-surface-area alumina) is the preferred catalyst for semi-hydrogenation of alkyne (e.g. ethyne, propyne) and alkadiene (e.g. propadiene, butadiene) impurities to olefins in C2–C5+ fractions of steam crackers [2,4,6–8]. 'Bare' Pd catalysts experience over-hydrogenation to the alkane and formation of higher hydrocarbons by oligomerization (green oil). Accordingly, modification of monometallic Pd systems by promoters and/or additives is essential to increase the alkene selectivity and lifetime [3,5,8,9]. A representative example of modified palladium catalyst for partial hydrogenation of triple bonds in the fine chemical industry is the Lindlar system, consisting of 5 wt% Pd supported on $CaCO_3$ promoted by lead diacetate and quinoline [10]. Compared to palladium catalysts, supported nickel catalysts prepared by impregnation are more selective to the alkane while displaying extensive oligomerization [7,8,11,12]. In fact, nickel is frequently used for alkene hydrogenation or total alkyne hydrogenation [1,3]. Besides, nickel requires higher operating temperatures (up to 623 K) than palladium (323–353 K) [1]. Strategies to prevent total hydrogenation over nickel catalysts include promotion by additional metals (e.g. Cu, Re, Pb, Ag, Bi, Mo) [7,13,14], partial presulfiding, and continuous dosing of small H_2S amounts to the reactor [1].

Pd has monopolized recent open-literature publications on hydrogenation of alkynes, dienes, and alkenes [5,15–19], which was traditionally focused on supported nickel (on alumina or pumice), Raney nickel, and nickel boride catalysts [20–26]. Supported gold nanoparticles also attract recent attention due to the superior thermodynamic selectivity with respect to palladium [27]. In the nineties, Monzón et al. [28] prepared $Ni/NiAl_2O_4$ by coprecipitation of Ni_1–Al_2 precursors (22 wt% Ni) followed by calcination at 1173 K and reduction at 773 K. Tests in ethyne hydrogenation at 423 K led to very low ethene yields (ca. 6%) and an extremely high coking rate (up to 7.5 $g_{coke}\, g_{cat}^{-1}\, h^{-1}$). Incorporation of Zn, Cr, and/or Fe in the base Ni_3–Al_1 hydrotalcite increased the ethene yield to 13% [29,30].

* Corresponding author at: Institute of Chemical Research of Catalonia (ICIQ), Avinguda Països Catalans 16, 43007 Tarragona, Spain. Fax: +34 977 920 224.
E-mail address: jperez@iciq.es (J. Pérez-Ramírez).

0021-9517/$ – see front matter © 2008 Elsevier Inc. All rights reserved.
doi:10.1016/j.jcat.2008.07.012

In general, hydrogenation studies of acetylenics and dienes over nickel catalysts used a fixed condition for activation of the precursor material (calcination and reduction) and catalytic tests have been typically conducted with ethyne [12,20,26,31,32]. Comprehensive relationships between the catalyst synthesis, structure, procedure for catalyst evaluation, and the resulting hydrorefining performance have not been derived. Besides, studies assessing the sensitivity to the hydrocarbon in terms of chain length (e.g. ethyne and propyne) and type of insaturation (e.g. propyne and propadiene) have not been reported. Monzón et al. [28] showed that the degree of nickel reduced can be controlled by the reduction temperature of the Ni–Al oxide, but the influence thereof on ethyne hydrogenation was not examined. Phillipson et al. [25] observed that the isomer selectivity in the hydrogenation of 1,3-butadiene is affected by the reduction temperature of Ni/Al_2O_3. Apart from reduction conditions, well established is also that the calcination of nickel oxide impacts on the reduction properties, as early shown by Benton and Emmett [33]. Consequently, the possibility rises to design rules for more efficient nickel-based hydrogenation catalysts by proper selection of the synthesis and activation conditions.

Herein, we have investigated *unpromoted* reduced Ni–Al mixed oxides derived from takovite (Ni–Al hydrotalcite) in the gas-phase hydrogenation of ethyne, propyne, and propadiene. The hydrotalcite route makes it possible to obtain multimetallic mixed oxides combining high metal loadings, high metal (inter)dispersion, and high surface area [34–36]. Structure–performance relationships associated with the activation of the takovite precursor have been derived by detailed characterizations and catalytic tests in a continuous fixed-bed reactor at different temperatures and hydrogen-to-hydrocarbon ratios. *Operando* infrared spectroscopy monitored the formation of carbon-containing species on the catalyst surface under reaction conditions, which has been correlated with changes in alkene selectivity.

2. Experimental

2.1. Catalyst preparation and activation

Ni–Al hydrotalcite with a nominal Ni/Al molar ratio of 3, known as takovite, was synthesized by continuous coprecipitation using the ILDP method [37]. Briefly, aqueous solutions of 0.75 M $Ni(NO_3)_2{\cdot}6H_2O$ and 0.25 M $Al(NO_3)_3{\cdot}9H_2O$ and the precipitating agent ($NaOH + Na_2CO_3$, 1 M of each) were pumped into a 6 ml-microreactor attached to a high-shear homogenizer rotating at 13,500 rpm. The pH of the slurry was measured and controlled by an in-line probe directly at the outlet of the precipitation chamber. The synthesis was carried out at constant pH 10 with an average residence time of 18 s. The product slurry was collected in a glass vessel and aged at 313 K for 12 h under stirring, followed by filtration, washing, and drying at 353 K for 12 h. The as-synthesized sample, denoted as 'AS,' was calcined in static air at different temperatures (623, 773, or 1173 K) for 15 h using a ramp of 5 $K\,min^{-1}$. Previous to catalytic tests (Section 2.3), the calcined samples were treated in He at 623 K for 30 min and cooled or heated in the same gas to the desired prereduction temperature (423, 623, or 773 K), which was done in a mixture of 5 vol% H_2 in He during 30 min. Occasionally, a 5 h-reduction treatment was carried out. The ramp used in the temperature programs was 5 $K\,min^{-1}$. Along the manuscript, the samples are designated as 'C*x*–R*y*,' where '*x*' and '*y*' stand for the calcination and reduction temperatures, respectively.

2.2. Catalyst characterization

The chemical composition of the as-synthesized Ni–Al hydrotalcite was determined by X-ray fluorescence in a Philips PW 2400 spectrometer. Before analysis, the sample was mixed with $Li_2B_4O_7$ and LiI as tensoactive agent, and the mixture was fused at 1423 K in a Perle'X-3 radiofrequency furnace.

Powder X-ray diffraction was studied in a Brucker-AXS D5005 θ–θ diffractometer equipped with a Bruker-AXS MRI high-temperature chamber and a diffracted beam graphite monochromator using Cu$K\alpha$ radiation. A thin layer of sample (ca. 30 mg) was mounted on the Pt_{90}–Rh_{10} heater strip by placing a few droplets of a suspension of finely ground sample in ethanol followed by drying under ambient conditions. The as-synthesized and calcined samples were measured at 298 K in N_2 (100 ml STP min^{-1}). *In situ* XRD patterns during reduction of the Ni–Al oxides were recorded in 5 vol% H_2 in N_2 (100 ml STP min^{-1}) at 423, 623, 773, and 1173 K after 30 min equilibration at each temperature. The heating rate between each temperature step was 5 $K\,min^{-1}$. Data were collected at $2\theta = 10°$–$70°$ with a step size of 0.05° and a counting time of 1 s per step.

Thermal analysis was performed in a Mettler Toledo TGA/SDTA851e microbalance. Analyses were performed in air (50 ml STP min^{-1}), ramping the temperature from 298 to 1173 K at 5 $K\,min^{-1}$.

N_2 isotherms at 77 K were measured in a Quantachrome Autosorb-1 MP analyzer. Before analysis, the samples were degassed in vacuum at 393 K for 12 h.

Temperature-programmed reduction with hydrogen (H_2-TPR) was measured in a Thermo TPDRO 1100 unit equipped with a thermal conductivity detector. Ca. 50 mg of Ni–Al oxide obtained by calcination of takovite at 623, 773, and 1173 K were loaded in the quartz microreactor (11 mm i.d.), pretreated in N_2 (20 ml STP min^{-1}) at 623 K for 1 h, and cooled to 323 K in the same atmosphere. The analysis was carried out in a mixture of 5 vol% H_2 in N_2 (20 ml STP min^{-1}), ramping the temperature from 323 to 1173 K at 10 $K\,min^{-1}$. H_2-TPR was also carried out over prereduced samples. For this purpose, the calcined samples were *in situ* reduced in 5 vol% H_2 in N_2 (42 ml STP min^{-1}) at different temperatures (423, 623, and 773 K) and times (30 min and 5 h) previous to the analysis.

X-ray photoelectron spectroscopy (XPS) measurements were obtained using a VG-Microtech Multilab 3000 spectrometer equipped with a Mg$K\alpha$ ($h\nu = 1253.6$ eV) excitation source, a nine-channeltron detection system, and a hemispheric electron analyzer. The sample was outgassed overnight at room temperature in a UHV chamber ($<5 \times 10^{-8}$ Torr). In some cases, before XPS measurements, the specimen was transferred to a high-pressure reaction cell (10^{-3} Torr) attached to the analysis chamber of the spectrometer and pretreated in H_2 at 773 K. Reduced samples were immediately transferred to the analysis chamber. All binding energies were referenced to the C 1*s* line at 284.6 eV, and the integrated intensities were corrected by atomic sensitivity factors [38].

2.3. Catalytic tests

The gas-phase hydrogenation of propyne, propadiene, and ethyne was studied at ambient pressure in a MicroActivity Reference setup (PID Eng&Tech). The catalyst (0.15 g, sieve fraction 200–400 μm) was loaded in the 12 mm i.d. quartz microreactor, heated in He at 623 K for 30 min, and prereduced in 5 vol% H_2 in He (42 ml STP min^{-1}) as described in Section 2.1. The catalysts were tested isothermally at intervals of 50 K in the range 373–523 K using a typical feed mixture of (alkyne or alkadiene)/H_2/He = 2.5/7.5/90 and a total flow of 42 ml STP min^{-1} (weight hourly space velocity, WHSV = 16,800 ml h^{-1} g^{-1}). The tests were run starting at the highest or lowest temperature, with a holding time of 5 h at each temperature. The influence of the hydrogen-to-propyne ratio (1–5) was studied over selected catalysts at 523 K. For this purpose, the inlet hydrocarbon concentration was kept at 2.5 vol% and the hydrogen concentration was decreased from 12.5 to 2.5 vol%

by balancing the mixture with He in order to keep the total flow constant. The product gases were analyzed by a gas chromatograph (Agilent GC6890N) equipped with a GS-GasPro column and a thermal conductivity detector. The turnover frequency was expressed as [mole alkyne/alkadiene converted $\cdot s^{-1} \cdot$ mole Ni reduced^{-1}]. The selectivity to the alkene (alkane) was determined as the mole of alkene (alkane) formed divided by the mole of propyne, propadiene, or ethyne reacted. The alkene yield was determined as the product of alkyne (alkadiene) conversion and alkene selectivity. The fractional selectivity to oligomers (often referred to as green oil) was determined as $S(\text{oligomers}) = 1 - S(\text{alkene}) - S(\text{alkane})$.

2.4. Operando FTIR spectroscopy

Fourier transform infrared spectroscopy was carried out in a Nicolet 5700 spectrometer (Thermo Scientific) using a Spectratech collector II diffuse reflectance (DRIFT) accessory equipped with a high-temperature chamber, ZnSe windows, and a MCT detector. The sample cell was filled with powdered catalyst and carefully leveled off to reduce reflections off the sample surface and to ensure reproducible results. The experiments were carried out reproducing the procedures detailed in Section 2.3. Gases were dosed into the cell by digital mass flow controllers. Spectra were automatically recorded every 80 s during 5 h using KBr (Aldrich, IR spectroscopy grade) under reaction conditions as the background. The range 650–4000 cm^{-1} was covered by co-addition of 32 scans at a nominal resolution of 4 cm^{-1}.

3. Results and discussion

3.1. Hydrotalcite activation

3.1.1. As-synthesized sample

Fig. 1 shows the XRD patterns of the coprecipitated material and the products of calcination and reduction at different conditions. The as-synthesized sample (AS) presents characteristic reflections of takovite ($Ni_6Al_2(OH)_{16}CO_3{\cdot}4H_2O$, JCPDS 15-0087). The molar Ni/Al ratio in the solid determined by XRF (3.3) was close to the nominal ratio of 3. Takovite had the platelet-like morphology characteristic of hydrotalcite-type compounds [34,39] (Fig. S1 in Supplementary information). The sample was purely mesoporous, with a total pore volume of 0.32 cm^3 g^{-1} and a BET surface area of 227 m^2 g^{-1}. Thermogravimetric analysis in air (Fig. 2) shows the typical two-step decomposition pattern of these clays [39], with transition temperatures at 375 K (interlayer water removal) and 570 K (dehydroxylation and decarbonation).

3.1.2. Calcination

As shown in Fig. 1 and summarized in Table 1, the XRD patterns of the materials calcined at 623 and 773 K showed NiO (bunsenite, JCPDS 47-1049), while both NiO and $NiAl_2O_4$ spinel coexist in the material calcined at 1173 K. No distinctive reflections associated with any crystalline form of alumina were detected in the samples. The nickel and aluminum content in the oxides is 58 wt% and 8 wt%, respectively. In agreement with the literature [39–41], the NiO reflections in the calcined samples were shifted to higher 2θ values than those corresponding to pure NiO, due to Al^{3+} substitution in the nickel oxide lattice and the formation of a solid solution, denoted as Ni(Al)O_x. Puxley et al. [42] described this solid solution as a highly disordered metastable mixed oxide, intermediate in nature between pure nickel oxide and nickel aluminate. Hence, the cubic cell of the solid solution in C623 and C773 ($a = 0.4151$–0.4157 nm) is significantly smaller than that of NiO ($a = 0.4177$ nm, JCPDS 47-1049). In line with our results, Alzamora et al. [40] reported similar d spacings for the hydrotalcite-derived Ni–Al oxides calcined at 573 and 723 K.

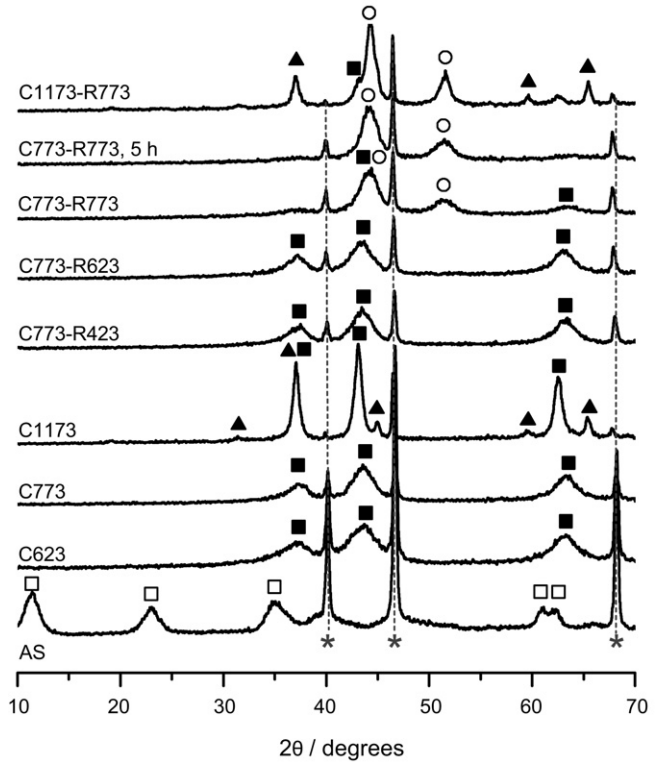

Fig. 1. XRD patterns of the as-synthesized takovite and the products of calcination and *in situ* reduction at different conditions. Crystalline phases: (□) takovite, (■) NiO, (▲) $NiAl_2O_4$ and (○) Ni. The reflections with asterisk belong to the Pt_{95}–Rh_5 strip where the samples were mounted.

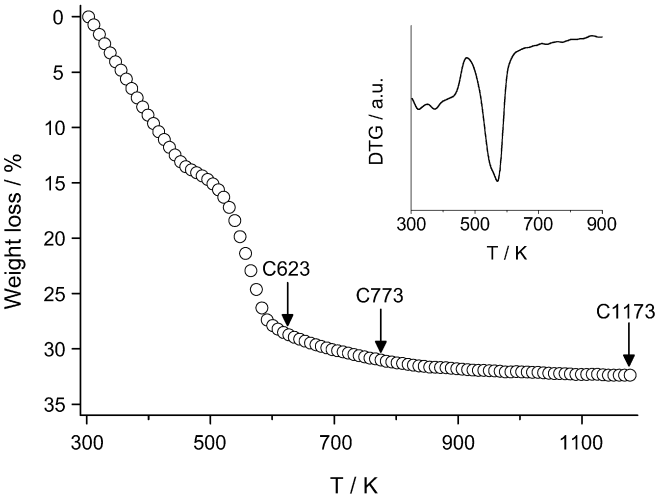

Fig. 2. Thermogravimetric profile of the as-synthesized takovite in air and derivative of the weight loss (inset).

The cell parameter of the NiO phase in C1173 ($a = 0.4171$ nm) resembles that of pure nickel oxide, suggesting that at this calcination temperature aluminum is segregated from the solid solution forming the additional $NiAl_2O_4$ spinel phase. It has been reported that at ca. 1073 K, Ni(Al)O_x starts to transform into additional phases, namely $NiAl_2O_4$ [42]. Both nickel oxide and nickel aluminate present a cubic close-packed lattice of O^{2-} ions, only differing in the way in which the cation vacancies are filled. Ni^{2+} ions occupy octahedral sites in NiO and tetrahedral sites in the normal spinel $NiAl_2O_4$, respectively. The concentration of nickel in

Table 1
Characterization data of the takovite-derived samples

Sample code[a]	Phases[b]	Ni reduced[c] (%)	S_{BET} ($m^2\,g^{-1}$)
C623	NiO	–	275
C773	NiO	–	206
C1173	NiO + $NiAl_2O_4$	–	62
C623–R423	NiO	0	250
C623–R623	NiO	17	238
C773–R423	NiO	0	178
C773–R623	NiO	6	170
C773–R773	NiO + Ni	55	155
C773–R773, 5 h[d]	NiO + Ni	91	166
C1173–R773	NiO + $NiAl_2O_4$ + Ni	37	55

[a] C and R stand for calcination and reduction treatments, respectively. The numbers indicate the temperature in K.
[b] Identified by XRD.
[c] Percentage of metallic nickel determined by H_2-TPR.
[d] Reduced for 5 h. Reduction time in the other samples was 30 min.

T_d sites increases with temperature (>1273 K). At lower temperature, due to the preference of Ni^{2+} ions for octahedral sites, an inverse nickel aluminate spinel is favored [43]. Accordingly, both NiO and $NiAl_2O_4$ with different degrees of inversion coexist in C1173. Besides, as revealed by H_2-TPR (*vide infra*), a certain amount of Ni(Al)O_x still remains in this sample.

The samples calcined at 623 and 773 K present no appreciable differences in average crystallite size (ca. 3 nm), as determined by the Scherrer method using the (220) reflection at $2\theta = 63°$. Calcination at 1173 K leads to larger NiO crystallites (ca. 8 nm). The average crystallite size of the $NiAl_2O_4$ spinel in C1173 amounted to 16 nm (estimated using the (440) reflection at $2\theta = 65°$). The morphology of these oxides was studied by TEM. Representative micrographs are shown in Supplementary information. Uniform nanoparticles of ca. 10 nm were observed in C773. The sample calcined at 623 K combines platelets inherited from the as-synthesized material and small nanoparticles (3–5 nm) characteristic of the oxide. The transformation from lamellae in Ni–Al hydrotalcite to nodular particles in the corresponding oxide was reported elsewhere [39,44]. In agreement with XRD, C1173 presents larger particles, in the range of 10–25 nm, due to sintering of NiO and crystallization of $NiAl_2O_4$. Nitrogen adsorption reveals the progressive decrease of BET surface area upon increasing the calcination temperature, particularly at 1173 K (Table 1). Alzamora et al. [40] also showed that the segregation of aluminum from the Ni(Al)O_x solid solution and subsequent crystallization of the $NiAl_2O_4$ spinel causes a drastic drop in surface area.

3.1.3. Reduction

H_2-TPR was used to investigate the influence of the calcination temperature on the reducibility of nickel in the samples and to design prereduction treatments for deriving relationships between the amount of nickel reduced and the hydrogenation performance (Section 3.2). As shown in Fig. 3, the reduction of nickel occurs in the broad range of 600–1050 K depending on the calcination temperature of the takovite precursor. The unreduced C623 sample shows a peak of hydrogen consumption centered at 800 K, with a small peak at 645 K and a shoulder at 925 K. The unreduced C773 sample shows a more symmetrical profile centered at 925 K without the low-temperature contribution.

Pure NiO obtained by calcination of nickel nitrate at 773 K typically displays a single peak consumption at 673 K [45,46], more or less matching the low-temperature peak in C623. The reduction of nickel in Ni(Al)O_x solid solutions is hindered by aluminum [41], causing the shift to higher temperatures. The reduction temperature increases significantly from C623 (peak at 800 K) to C773 (peak at 925 K), strongly suggesting that the interaction of aluminum and nickel in the solid solution is enhanced in the latter sample. This might be due to the favored solid-state diffusion of

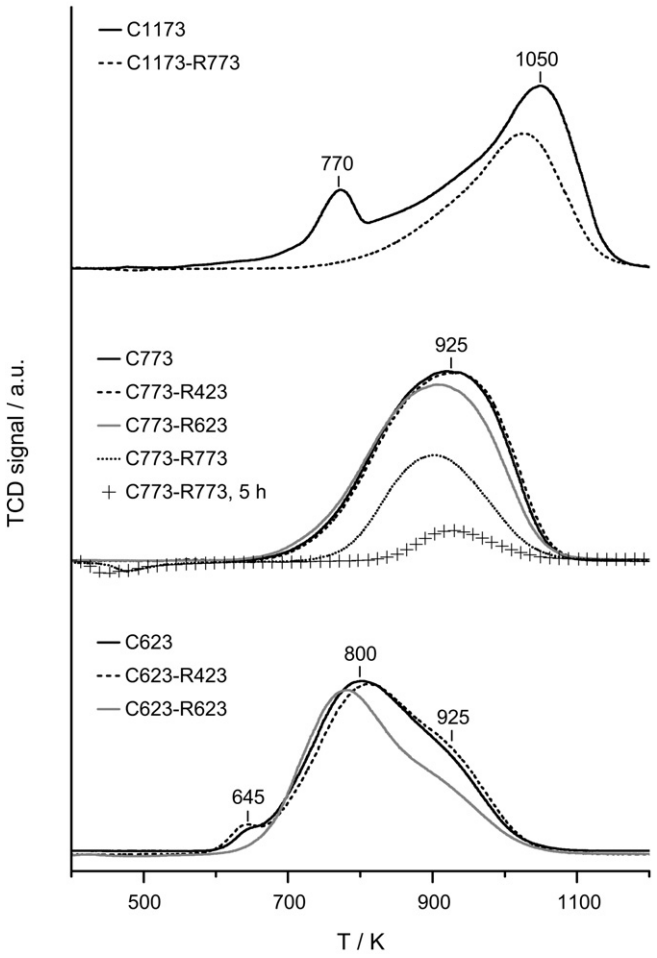

Fig. 3. H_2-TPR profiles of the Ni–Al catalysts calcined and reduced at different conditions.

aluminum in the NiO lattice. The broad reducibility range in C623 and C773 is likely due to the presence of nickel species in different environments in terms of interaction with aluminum. This substantiates the presence of a multiple range of structures in the model by Puxley et al. [42].

It is well known that the presence of Al^{3+} in nickel oxide increases the resistance of Ni^{2+} against reduction [39,42]. In analogy with the work by Arnoldy and Moulijn [47] over the Co–Al system, the number of Al^{3+} ions in the surrounding of the Ni^{2+} ion should mainly determine the reduction temperature. Al^{3+} ions exert a ligand effect, polarizing the more or less covalent Ni–O bonds, thus increasing the effective charge of Ni^{2+} ions, and as a consequence, the lattice energy, resulting in a higher reduction temperature of the intermediate Ni(Al)O_x phases as compared to NiO.

In the unreduced C1173 sample, the peak centered at 925 K in C773 is unfolded in two peaks at 770 and 1050 K. The low-temperature peak corresponds to NiO generated upon withdrawal of aluminum from the Ni(Al)O_x solid solution, while the high-temperature peak is attributed to the incipient $NiAl_2O_4$. The H_2 consumption by NiO is much lower than that by $NiAl_2O_4$, which does not account for the total segregation of aluminum from the solid solution [41,48,49]. With a nominal Ni/Al ratio in the solid of 3, the theoretical molar ratio NiO/$NiAl_2O_4$ is 5. Thus, a wide range of oxidic structures coexist in this sample too, namely NiO, Ni(Al)O_x, and $NiAl_2O_4$, covering the broad range of 800–1200 K.

H_2-TPR was also carried out over *in situ* reduced samples using different temperature and time. The prereduction temperature of the samples never exceeded the calcination temperature. As shown

in Fig. 3, pretreatment of C623 in H_2 at 423 K did not produce detectable reduction of nickel species, while increasing the temperature to 623 K led to the disappearance of the small peak at 645 K, attributed to free NiO. The area of the broad peak at 800 K is somewhat decreased and slightly shifted to lower temperatures. A similar behavior was observed for the C773 sample: prereduction at 423 K originated no change and the peak area gradually decreased by H_2 pretreatment at 623 and 773 K. The reduction was particularly significant in the sample treated for 5 h. In the same line, H_2 pretreatment of C1173 at 773 K resulted in the disappearance of the peak at 770 K due to complete NiO reduction, and the decreased area of the peak at 1050 K is mainly due to nickel reduction in Ni(Al)O_x phases, while Ni^{2+} in the spinel phase is unreduced. The latter reasoning is grounded on the practically unchanged XRD reflections of the $NiAl_2O_4$ phase upon reduction (Fig. 1).

The fraction of metallic nickel was determined dividing the total integral area of the prereduced samples by that of the unreduced counterparts (Table 1). As expected, (i) the amount of reduced Ni at a fixed calcination temperature increases with the prereduction temperature (compare the C773–R*y* series) and (ii) higher calcination temperature requires higher prereduction temperature to reach an equivalent percentage of metallic nickel (compare C623–R623 and C773–R623 or C773–R773 and C1173–R773). In light of these results, it can be concluded that the degree of bulk nickel reduction in the oxide can be modulated by adjusting temperature and time. For example, the amount of Ni^0 in C773 is 0, 6, and 55% upon prereduction at 423, 623, and 773 K for 30 min, respectively, reaching 91% when the prereduction time at 773 K was 5 h.

H_2-TPR results agree with *in situ* XRD studies during reduction of the C773 sample (Fig. 1). The intensity of the NiO diffraction lines in C773 and C773–R423 is virtually the same, and is slightly reduced in C773–R623. Reflections of metallic Ni were not observed in these samples. The intensity of NiO in C773–R773 significantly decreased and two broad reflections belonging to Ni^0 (JCPDS 4-850) emerged at $2\theta = 44°$ and 52°. The degree of nickel reduction in C773–R773 was estimated as the ratio of the area of the NiO (220) reflection at $2\theta = 63°$ and the area of the same reflection in unreduced C773. The resulting value (57%) is in excellent correspondence with that determined by H_2-TPR (55%, Table 1). Based on the (220) reflection, no NiO was identified in the C773–R773 sample reduced for 5 h due to the complete nickel reduction. The XRD pattern of C1173–R773 shows the virtual disappearance of NiO, while $NiAl_2O_4$ reflections are still present, though exhibiting a lower intensity compared to C1173. The average size of the nickel crystallites in these reduced samples was estimated by the Scherrer method applied in the Ni (200) reflection at $2\theta = 52°$. As expected, Ni^0 crystallites in C773–R773 (3 nm) are smaller than in C1173–R773 (6 nm) since the size of the metal is very much inherited from the crystallite size of the nickel oxide precursor.

Finally, transmission electron microscopy and nitrogen adsorption were carried out in order to check whether the reduction treatments affect the morphological and textural properties of the precursor oxides. The morphology of the calcined and reduced samples did not apparently change (Supplementary information). The reduction treatments did not significantly alter the BET surface area of the samples either (Table 1).

3.1.4. Surface vs bulk analyses

The bulk analyses presented above, namely XRD and H_2-TPR, indicated that the oxide resulting from calcination of takovite at 773 K consisted of a Ni–Al solid solution. However, these techniques provide no insight on the chemical state of nickel on the surface and the aluminum distribution within the catalyst particle. For this purpose, XPS analysis was carried out over C773 and C773–R773 (Fig. 4 and Table 2). The latter is the best hydrogenation catalyst identified in our study (see Section 3.2). The Ni $2p_{3/2}$ core level spectrum of C773 shows a binding energy of 855.6 eV and the corresponding shake-up satellite at ca. 6 eV above the principal line [50]. This peak, characteristic of Ni^{2+}, is positioned between the binding energy of NiO (854.1 eV [51]) and $NiAl_2O_4$ spinel (856.2 eV [52]). This further indicates the intimate interaction of Ni^{2+} and Al^{3+} in the catalyst, pointing once more to the presence of metastable phases intermediate in nature between the two structures. Noticeably, the atomic Ni/Al ratio of C773 determined by XPS amounts to 1.4, i.e. much lower than the bulk Ni/Al ratio of 3.3 determined by XRF (Table 2). Consequently, the surface of the oxide is enriched by aluminum. Various authors have reported aluminum zoning on the surface of Ni–Al oxides derived from thermal treatment of Ni–Al hydrotalcite [40,41,53]. For example, based on alkaline leaching coupled with ^{27}Al MAS-NMR analyses, Rebours et al. [53] concluded that the oxide at 923 K consists of NiO particles whose surface is decorated by aluminate-type patches.

The Ni $2p_{3/2}$ core level spectrum of C773–R773 displays an additional peak at 852.9 eV, which is assigned to Ni^0 [54], although the peak due to Ni^{2+} is still predominant (Fig. 4). By peak deconvolution and taking into account the corresponding satellite peaks, it was determined that only 15% of the nickel probed by XPS is in metallic form. The amount of nickel reduced on the surface is much lower than that of 55% determined in the bulk (Table 2).

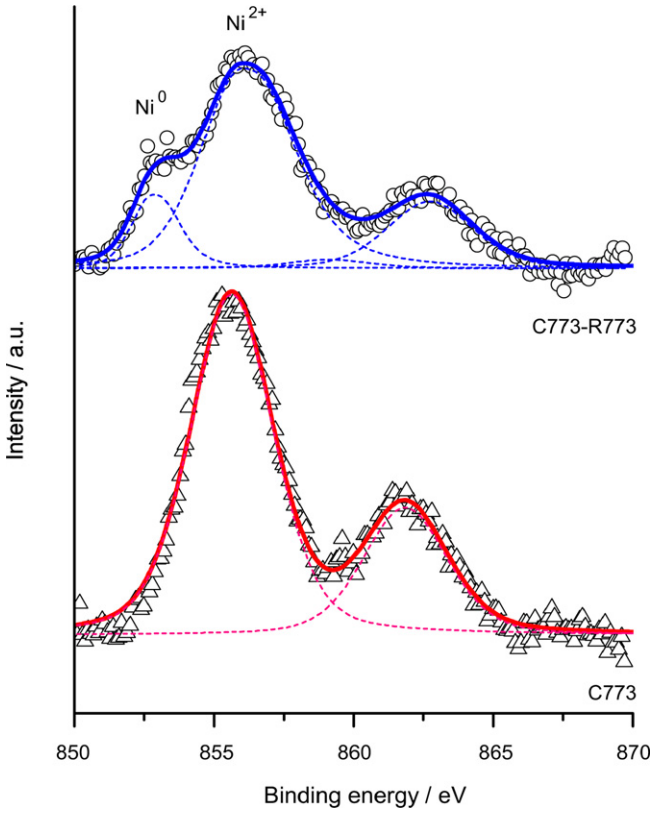

Fig. 4. Ni $2p_{3/2}$ core level spectrum of the C773 and C773–R773 samples.

Table 2
Comparative results of bulk and surface analyses over selected samples

Sample	Molar Ni/Al ratio (–)		Ni reduced (%)	
	XRF	XPS	H_2-TPR	XPS
C773	3.3	1.4	0	0
C773–R773	3.3	1.0	55	15

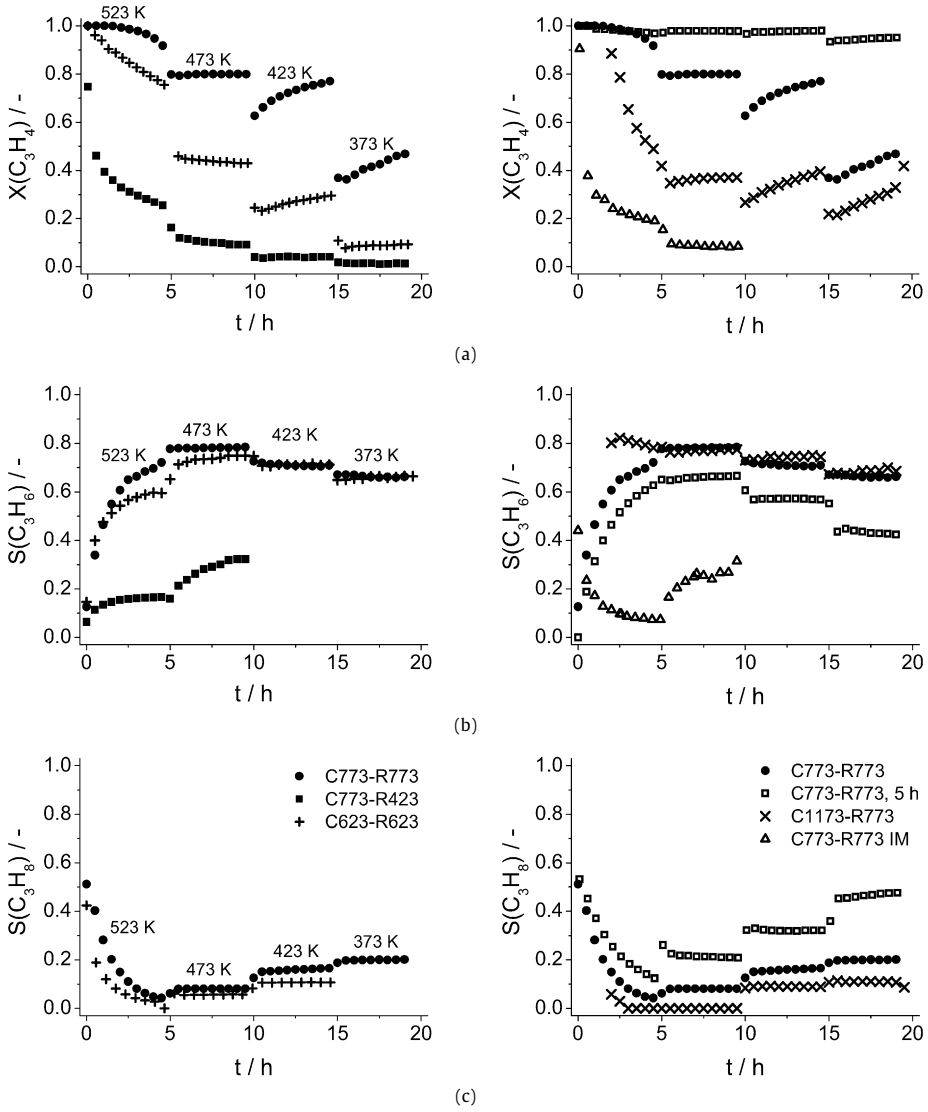

Fig. 5. Propyne conversion (a), propene selectivity (b), and propane selectivity (c) vs time during propyne hydrogenation over the Ni–Al catalysts. Conditions: $C_3H_4/H_2/He$ ratio = 2.5/7.5/90, $T = 373$–523 K, WHSV = 16,800 ml g^{-1} h^{-1}, and $P = 1$ bar.

This result can be tentatively explained considering the marked aluminum zoning, hindering more significantly nickel reduction at the surface of the catalyst. The atomic Ni/Al ratio in C773–R773 determined by XPS was 1.0 (Table 2), indicating that the reduction treatment enhances the relative enrichment of the surface by aluminum with respect to the calcined material. It has been suggested that the reduction of the samples causes the progressive diffusion of aluminum ions to the surface of the crystallite [40]. Finally, the Ni^{2+} contribution in XPS is shifted to higher binding energies upon reduction of the sample (856.3 eV in C773–R773 and 855.6 eV in C773), further accentuating the stronger interaction of Ni^{2+} and Al^{3+} in the solid solution upon partial reduction. This is due to both the higher surface concentration of aluminum and the lower Ni^{2+}/Al^{3+} ratio in the oxide upon Ni^0 formation, provoking that the ligand effect of Al^{3+} is distributed over a relatively lower number of Ni^{2+}.

3.2. Hydrogenation performance

3.2.1. Calcination and reduction conditions

Fig. 5 shows the propyne hydrogenation performance of the takovite-derived catalysts calcined and prereduced at different conditions. These tests were run at intervals of 50 K from 523 to 373 K. Tests from the lowest to the highest temperature were also conducted and have a strong impact on the catalytic performance. This aspect deserves a separate discussion (Section 3.3). The propene selectivity greatly increased with time-on-stream in the first 2 h of reaction at 523 K (Fig. 5b), with a concomitant decrease of propane selectivity (Fig. 5c) and propyne conversion (Fig. 5a). After this period, the catalysts display stable performance. As expected, the degree of propyne conversion decreases with decreasing temperature (Fig. 5a). The propene selectivity does not experience a marked dependence with temperature, although a slight decrease when going from 523 to 373 K is generally observed. The increase in propene selectivity at the beginning of the reaction was more pronounced over C773–R773, going from 0 to 50% in the first 2 h and reaching ca. 80% after 5 h on stream. In this period, the propane selectivity decreased from 50 to <5%. Monzón et al. [30, 55] attributed this behavior to the presence of two types of active sites in the nickel catalyst: hydrogenolytic (leading to the alkane) and hydrogenating (leading to the alkene). According to these authors, the former sites experienced fast deactivation by coke in ethyne hydrogenation, decreasing the alkane production. However, we cannot exclude the presence of a single type of sites in the catalyst that is *transformed* in early stages of the reaction, e.g. by formation of C-containing deposits on the surface, thereby mini-

mizing the pathway to the alkane. More details in this respect can be found in Section 3.3.

The hydrogenation performance over the Ni–Al catalysts is determined by (i) the nature of the oxidic nickel phase (determined by the calcination conditions) and (ii) the amount of metallic nickel (induced by the reduction conditions). The propene selectivity over most catalysts is in the range 60–80%. In general, the calcination temperature has a stronger influence on the alkyne conversion. Calcination at low temperature (623 K) is not appropriate due to the fact that the degree of required metallic Ni to attain high and stable propyne conversion is limited. On the other extreme, high calcination temperatures (1173 K) cause low propyne conversion due to extensive NiO sintering and formation of $NiAl_2O_4$. The prereduction treatment strongly depends on selecting an appropriate calcination temperature. The C773–R423 sample led to low propyne conversion (ca. 30% at 523 K) and propene selectivity (ca. 30% at 473 K) since this sample was virtually unreduced (Table 1). The lower activity of the latter sample with respect to the C623–R623 catalyst is explained by the hindered nickel reducibility attained by the diffusion of aluminum to the surface when the calcination temperature increases. As expected, increasing the prereduction temperature from 423 to 773 K guarantees a sufficient amount of active Ni^0 sites for hydrogenation. Extending the prereduction treatment from 30 min to 5 h results into the highest propyne conversion, ca. 100% in the temperature range studied, but this is accompanied by decreased propene selectivity. Overall, the best catalyst was C773–R773, displaying a C_3H_6 yield of 65%. To evaluate the importance of the synthesis route, a Ni/Al_2O_3 catalyst was prepared by incipient wetness followed by calcination and reduction at 773 K (C773–R773 IM). This sample, whose characterization is provided in Supplementary information, showed much lower propyne conversion and propene selectivity (C_3H_6 yield ∼6%).

The dependence of the average values of propyne conversion and products selectivity on the degree of nickel reduction determined by H_2-TPR is shown in Fig. 6a for the catalysts calcined at 773 K and reduced at different conditions (temperature and time). The propyne conversion increases with the percentage of metallic nickel in the samples, although the specific activity per mol of Ni^0 (turnover frequency, TOF) experiences an opposite trend (Fig. 6b). The mildly reduced C773–R623 sample (6% of nickel reduced) is ca. 5 times more active than the C773–R773 (55% of nickel reduced), although the TOF does not change at higher degrees of Ni reduction. The propane selectivity increases with the percentage of metallic nickel in the samples and the opposite occurs with the selectivity to oligomers. The volcano-type dependence of the propene selectivity indicates that an optimal degree of bulk reduction (ca. 55% in C773–R773) maximizes the $S(C_3H_6)$ at 80%. The maximum in propene selectivity is likely related to the existence of an optimum between the rate of hydrogenation and the rate of oligomerization [5]. The relative significance of these two paths controls the selectivity to the desired product. A low degree of Ni reduction induces a lower rate of hydrogenation due to the limited number of sites to dissociate H_2. Consequently, the recombination of neighboring intermediate hydrocarbon fragments into oligomers is favored. Contrarily, at high degrees of nickel reduction, (sub-)surface Ni-hydride species can be formed, increasing the alkyne conversion and the selectivity to the over-hydrogenated hydrocarbon.

3.2.2. Hydrogen-to-hydrocarbon ratio

The average values of propyne conversion and products selectivity over the optimal C773–R773 catalyst using feed H_2-to-propyne ratios ranging from 5 to 1 and 523 K are shown in Fig. 7. The pattern in this figure qualitatively resembles those obtained with the different degree of nickel reduction in Fig. 6. The propyne con-

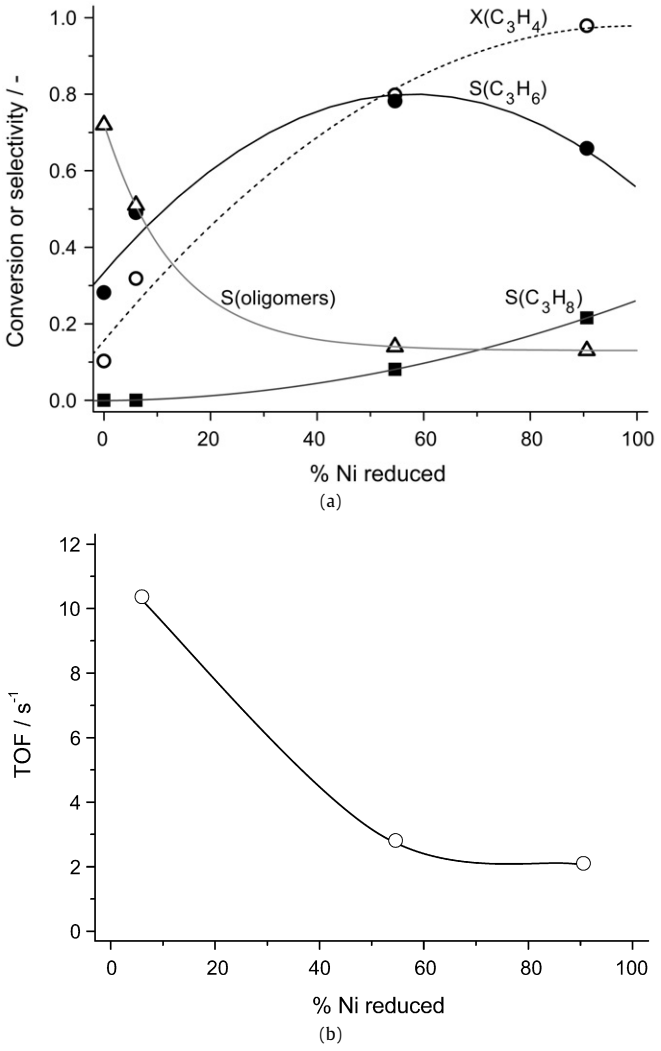

Fig. 6. Conversion of C_3H_4 and selectivity to C_3H_6, C_3H_8, and oligomers (a) and turnover frequency (b) as a function of the percentage of metallic nickel in differently reduced C773 catalysts (see Table 1). Data represent averaged values of the 5 h reaction period at 473 K in Fig. 7. The TOF is expressed as mole C_3H_4 converted per second and mole of Ni^0.

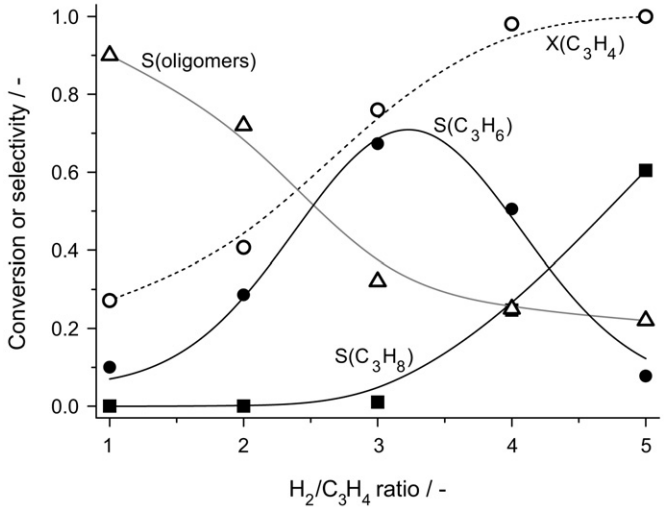

Fig. 7. Conversion of C_3H_4 and selectivity to C_3H_6, C_3H_8, and oligomers vs the feed hydrogen-to-propyne ratio over C773–R773. Conditions: $T = 523$ K, WHSV = 16,800 ml g^{-1} h^{-1}, and $P = 1$ bar.

version increases on increasing the partial pressure of H_2 at the reactor inlet, since the reaction rate is largely governed by the high concentration of adsorbed hydrogen atoms and nickel hydride species [8]. The hydrogenation of alkenes and alkynes has been classically described by the Horiuti–Polanyi mechanism [56], consisting of the successive addition of atomic hydrogen to the substrate. The selectivity to propane increases with the H_2/C_3H_4 ratio and the selectivity to oligomers displays the opposite trend. A high coverage of hydrogen favors total hydrogenation, while low hydrogen coverage favors oligomerization of the adsorbed hydrocarbon [57]. At high partial H_2 pressure, the eventual formation of a nickel hydride phase could account for the high C_3H_8 production. Analogously, high H_2/HC ratios over palladium catalysts form the hydrogen-saturated β-hydride phase, which is highly reactive but unselective [5,19]. In consequence, there is an optimal hydrogen pressure at which the selectivity to the partially hydrogenated product is maximized. The propene selectivity over C773–R773 was ca. 70% at $H_2/C_3H_4 = 3$ and the selectivity to oligomers was ca. 30% (i.e. no alkane was produced). Going slightly over or below this optimal ratio causes a significant decrease of the olefin selectivity.

3.2.3. Sensitivity to the hydrocarbon

We have assessed whether the promising catalytic results using propyne can be extrapolated to related unsaturated hydrocarbons such as ethyne and propadiene. The performance of selected catalysts in the hydrogenation of propyne, propadiene, and ethyne is compared in Fig. 8. Average values of conversion, selectivity, and yield at 473 K were plotted, since the catalysts exhibited stable performance at this temperature. The results indicate the superior activity of the Ni–Al catalysts in the hydrogenation of both propyne and propadiene as compared to ethyne (Fig. 8a). The highest conversions were attained with propadiene, which is due to the high reactivity of the diene [8]. The conversion of propadiene is in the relatively narrow range of 65–80% despite marked differences in calcination and reduction of the samples. The selectivity to propene was significantly lower with propadiene than with propyne (Fig. 8b), due to favored oligomerization and certain propane formation over the former substrate. It has been previously suggested that during reaction over nickel catalysts, propadiene is converted into C6 products due to the isomerization of the half-hydrogenated product (2-propenyl), giving a free radical that can attack a neighboring adsorbed propadiene molecule [8,22]. Considering the stronger adsorption of an alkadiene with respect to a monoene, the lower C_3H_6 selectivity with propadiene can also be explained taking into account the higher probability of C–C bond formation if both terminal carbon atoms are susceptible of being fully hydrogenated. In general, and particularly for C773–R773, the C_3H_6 yield was higher using propyne (up to 62%) than propadiene (up to 47%).

In great contrast to the tests with C3s, ethyne hydrogenation led to extremely low alkyne conversion (<12%). The ethene selectivity was well measurable only over the C773–R773 catalyst, amounting to ca. 55%. This leads to a C_2H_4 yield of 6%, in excellent agreement with values over precipitated nickel catalysts reported by Peña et al. [28]. The gap between ethyne and propyne has been attributed to the extensive oligomerization with the C2 [5,8,12,21,24], causing very fast deactivation by coking and thus low ethene yields. The presence of the extra carbon of propadiene and propyne as compared to ethyne minimizes oligomer formation, as the steric hindrance prevents adjacent adsorption of the approaching molecule during the C–C bond forming step [5,8,21]. The more pronounced coking with ethyne was confirmed by thermogravimetric analysis of the used catalysts in air (Fig. 9). The total weight loss due to combustion of the carbonaceous deposits was higher in the catalyst subjected to ethyne hydrogenation

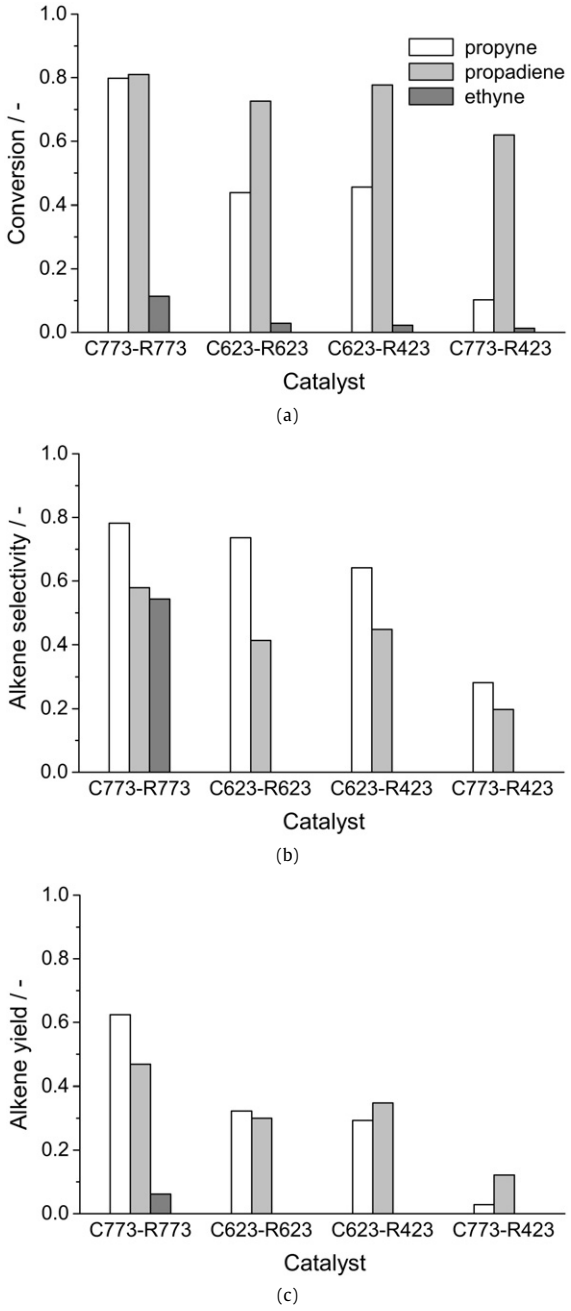

Fig. 8. Hydrocarbon conversion (a), alkene selectivity (b), and alkene yield (c) over selected catalysts in propyne, propadiene, and ethyne hydrogenation. Conditions: (C_3H_4 or C_2H_2)/H_2/He ratio = 2.5/7.5/90, $T = 473$ K, WHSV = 16,800 ml g^{-1} h^{-1}, and $P = 1$ bar.

(20%) compared to propyne and propadiene (15%). Interestingly, only one step of weight loss occurs in all the samples (transition temperature around 620 K), suggesting a similar nature of the coke deposits. N_2 adsorption revealed a lower surface area in the used catalysts due to coke residues. The BET surface area of the fresh C773–R773 catalyst (155 m^2 g^{-1}) markedly decreased to 77 m^2 g^{-1} after ethyne hydrogenation, while values of 128 and 115 m^2 g^{-1} were obtained after propyne and propadiene hydrogenation, respectively. Accordingly, ethyne should be used with extreme precaution to generally establish the potential of catalysts for hydrogenation of higher alkynes or dienes. Despite the marked performance differences among the substrates, the C773–R773 sample was the best catalyst for the three hydrocarbons investigated.

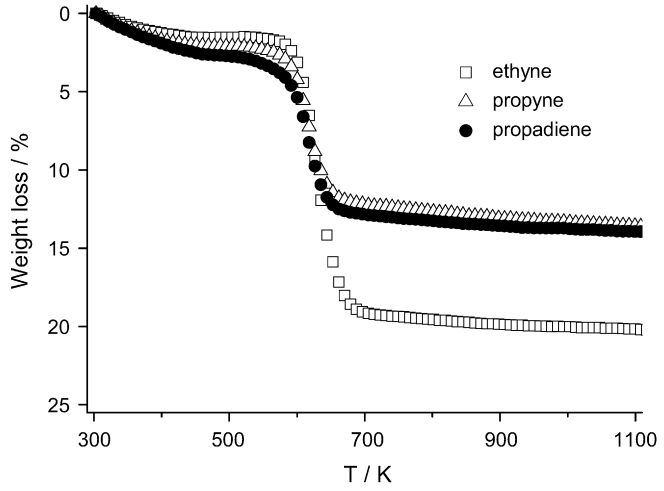

Fig. 9. TGA profiles in air of C773–R773 after hydrogenation of ethyne, propyne, and propadiene according to the test in Fig. 8.

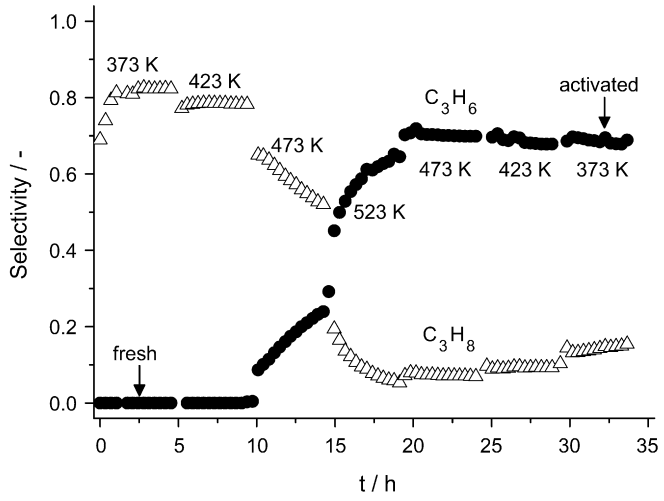

Fig. 10. Selectivity to propene and propane vs time during propyne hydrogenation over C773–R773. Conditions: C_3H_4/H_2/He ratio = 2.5/7.5/90, WHSV = 16,800 ml g^{-1} h^{-1}, and $P = 1$ bar. The temperature was increased stepwise from 373 to 523 K and then decreased back to 373 K.

3.3. Activation during reaction

Fig. 5 showed the pronounced increase of propene selectivity (from 0 to 70%) coupled to the decreased propane selectivity during the first stages of the reaction at 523 K. Afterwards, the $S(C_3H_6)$ is practically independent on the reaction temperature down to 373 K. The outcome of the test is spectacularly different if conducted from the lowest to the highest temperature. As shown in Fig. 10, the fresh C773–R773 catalyst shows a C_3H_8 selectivity of ca. 80% at 373 and 423 K, with no C_3H_6 production. At 473 K and more significantly at 523 K, the selectivity to propene increases at the expenses of propane, resembling the activation behavior in Fig. 5. As expected, once the catalyst is activated under reaction conditions, the propene selectivity does not change when going to lower temperature. This result highlights the importance of the testing procedure for the evaluation of hydrogenation catalysts and indicates that selectivity-enhancing species are formed in the specific temperature range of 473–523 K.

As previously reported over different metals [5,8,30,55,58], partial blocking of the surface by strongly held oligomers and coke deposits positively influenced the alkene selectivity during alkyne hydrogenation. Recently, it has been reported that dissolution of carbon (derived from fragmentation of alkyne molecules) in interstitial sites of Pd generates a metastable subsurface palladium carbide that turns the hydrogenation selective [19].

Further insights into the activation process, displayed over all substrates investigated here, were offered by *operando* infrared spectroscopy over the C773–R773 sample. Fig. 11 shows the evolution of the CH stretching region in infrared during propadiene hydrogenation at 523 K, which is indicative of the build up of C-containing deposits in the course of the reaction. Similar spectra were observed using propyne and acetylene (not shown for conciseness). The bands at 2960 and 2925 cm^{-1} are attributed to the asymmetric CH stretching of CH_3 and CH_2 groups, respectively [59,60]. The bands at 2871 cm^{-1} and the shoulder at 2856 cm^{-1} belong to the symmetric CH stretching of CH_3 and CH_2 groups, respectively. These bands were previously assigned to the formation of a carbonaceous layer on 2 wt% Pd/γ-Al_2O_3 on exposure to ethyne [60].

Fig. 12 shows the build up of C-containing deposits (obtained by integration and normalization of the infrared bands) during propadiene and ethyne hydrogenation and the corresponding C_3H_6 and C_2H_4 selectivity vs time-on-stream. The results with propyne were similar to those with propadiene. In agreement with the

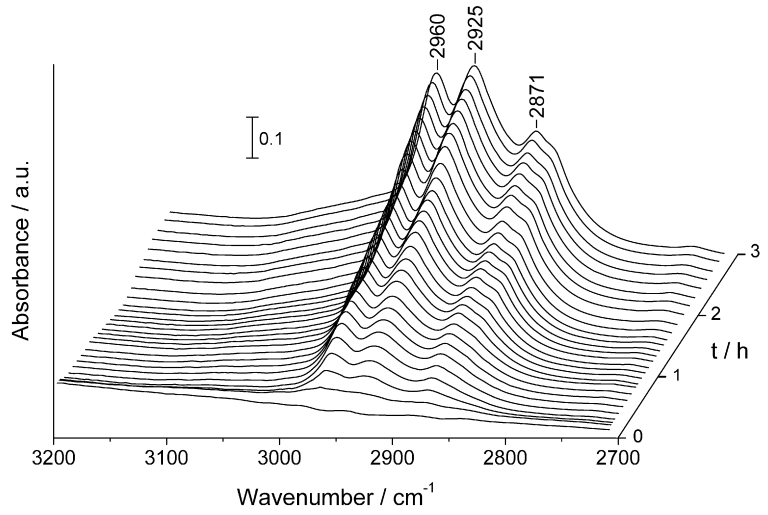

Fig. 11. *Operando* DRIFT spectra in the CH stretching region during propadiene hydrogenation over C773–R773. Conditions: C_3H_4/H_2/He ratio = 2.5/7.5/90, $T = 523$ K, WHSV = 16,800 ml g^{-1} h^{-1}, and $P = 1$ bar.

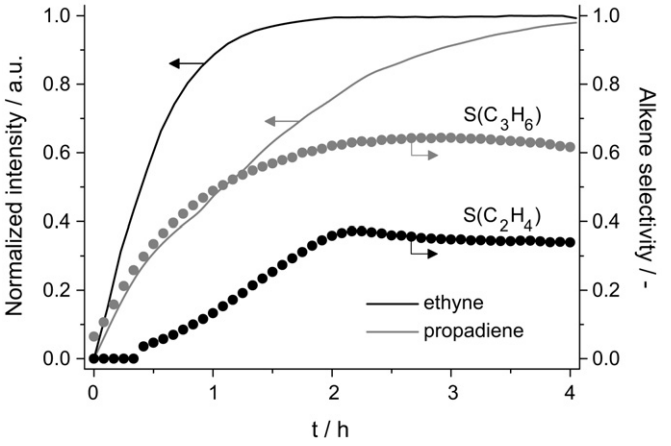

Fig. 12. Correlation between the normalized integral of the absorption bands in the 2800–3100 cm^{-1} range during *operando* DRIFT (lines) and the alkene selectivity (symbols) during propadiene and ethyne hydrogenation over C773–R773. Conditions: (C_3H_4 or C_2H_2)/H_2/He ratio = 2.5/7.5/90, $T = 523$ K, WHSV = 16,800 $ml\,g^{-1}\,h^{-1}$, and $P = 1$ bar.

higher tendency of ethyne to form oligomers (see Section 3.2.3), the development of the coke-related bands over the catalyst was remarkably faster compared to propadiene and propyne.

The increase in propene selectivity during propadiene hydrogenation correlates with the formation of carbonaceous deposits. On the other hand, the ethene selectivity increases slowly during the first two hours of reaction to ca. 40%, exhibiting a less evident relation with the coke build up determined by infrared spectroscopy. The formation of coke during ethyne hydrogenation does not facilitate an increase in alkene selectivity as strong as with propyne and propadiene. This suggests that the extensive coking process deactivates a significant fraction of active sites. This result is supported by the overall higher oligomer selectivity in this reaction (60% in the reaction with ethyne compared to 40% for propadiene).

Based on these results, it is plausible that the hydrogenation behavior of nickel is similar to that of palladium, in which the population of (sub-)surface sites governs the hydrogenation steps on the surface [19]. Consequently, nickel hydride-type species favor total hydrogenation. The latter species are not operative when surface C-containing deposits or even nickel carbide-type species are formed under certain reaction conditions, boosting the selectivity to the alkene. Further studies are required to ascertain the structure and nature of these species remain unclear, requiring further studies.

4. Conclusions

Reduced Ni–Al oxides obtained from takovite are highly active, selective, and stable catalysts for partial hydrogenation of propyne and propadiene, without addition of promoters. The intrinsic features of the hydrotalcite route in terms of attaining mixed oxides with high metal loadings, high metal (inter)dispersion, and high surface area are beneficial for the performance, which largely exceeds that of Ni/Al_2O_3 prepared by conventional impregnation. Proper selection of activation conditions of the takovite precursor (calcination and reduction of the derived mixed oxide) is decisive for the catalytic behavior, as they determine the nature of the oxide (crystalline phase structure, metal distribution, dispersion, and morphology) and the degree of nickel reduction. The best catalyst, calcined and reduced at 773 K, rendered stable propene yields up to ca. 65% and consisted of a $Ni(Al)O_x$ solid solution with 55% of the total bulk nickel in reduced form and surface enrichment by aluminum. Extensive sintering of NiO and crystallization of $NiAl_2O_4$ at high calcination temperature induce lower activity. The hydrocarbon conversion increases with the percentage of metallic Ni in the samples, while maximizing the monoalkene selectivity requires an optimal degree of nickel reduction. Over-hydrogenation occurs above the optimum, while oligomerization is favored below the optimum. The same pattern applies with the feed hydrogen-to-hydrocarbon ratio. *Operando* infrared spectroscopy gives evidence of the intimate relation between the increased alkene selectivity in early stages of the reaction and the formation of C-containing species on the catalyst (sub-)surface. These selectivity-enhancing species are formed at specific reaction temperatures, stressing the relevance of the testing procedure on assessing hydrogenation catalysts. In contrast with the C3s, ethyne hydrogenation led to much lower conversion and ethene selectivity as well as fast deactivation due to coking. Consequently, the latter should not be used as a model molecule to generally establish the potential of catalysts for hydrogenation of higher hydrocarbons.

Acknowledgments

This research was sponsored by the Spanish MEC (CTQ2006-01562/PPQ, PTQ05-01-00980, Consolider-Ingenio 2010: grant CSD-2006-00003) and the ICIQ Foundation. D.V. thanks the Erasmus programme for a fellowship. Dr. F. Coloma (Universidad de Alicante) is acknowledged for discussions on the XPS analyses.

Supplementary information

The online version of this article contains additional supplementary information.

Please visit DOI: 10.1016/j.jcat.2008.07.012.

References

[1] R.J. Farrauto, C.H. Bartholomew, Fundamentals of Industrial Catalytic Processes, Blackie Academic and Professional, London, 1997, p. 430.
[2] F. Cavani, F. Trifirò, Catal. Today 34 (1997) 269.
[3] H.F. Rase, Handbook of Commercial Catalysts, CRC Press, Boca Raton, 2000, p. 105.
[4] S. Nishimura, Handbook of Heterogeneous Catalytic Hydrogenation for Organic Synthesis, John Wiley and Sons, New York, 2001, p. 63.
[5] Á. Molnár, A. Sárkány, M. Varga, J. Mol. Catal. A 173 (2001) 185.
[6] M.L. Derrien, in: L. Červený (Ed.), Catalytic Hydrogenation, in: Stud. Surf. Sci. Catal., Elsevier, Amsterdam, 1986, p. 613.
[7] Y.J. Ryu, J.R. Adams, W.A. Groten, CA 02488051 (2004).
[8] G.C. Bond, Metal-Catalyzed Reactions of Hydrocarbons, Springer, New York, 2005, p. 395.
[9] N.A. Khan, S. Shaikhutdinov, H.-J. Freund, Catal. Lett. 108 (2006) 159.
[10] H. Lindlar, Helv. Chim. Acta 35 (1952) 446.
[11] J. Sheridan, J. Chem. Soc. (1945) 133.
[12] G.C. Bond, J. Chem. Soc. (1958) 2705.
[13] C. Trinh Dinh, J. Bournonville, US 4504593 (1984).
[14] H.M. Putman, J.R. Adams, WO 2006/08336 A2 (2006).
[15] E.W. Hansen, M. Neurock, J. Catal. 196 (2000) 241.
[16] E.W. Hansen, M. Neurock, J. Phys. Chem. B 105 (2001) 9218.
[17] D. Teschner, E. Vass, M. Hävecker, S. Zafeiratos, P. Schnörch, H. Sauer, A. Knop-Gericke, R. Schlögl, M. Chamam, A. Wootsch, A.S. Canning, J.J. Gamman, S.D. Jackson, J. McGregor, L.F. Gladden, J. Catal. 242 (2006) 26.
[18] W. Huang, W. Pyrz, R.F. Lobo, J.G. Chen, Appl. Catal. A 333 (2007) 254.
[19] D. Teschner, J. Borsodi, A. Wootsch, Z. Révay, M. Hävecker, A. Knop-Gericke, S.D. Jackson, R. Schlögl, Science 320 (2008) 86.
[20] J. Sheridan, J. Chem. Soc. (1944) 373.
[21] G.C. Bond, J. Sheridan, Trans. Faraday Soc. 48 (1952) 651.
[22] G.C. Bond, J. Sheridan, Trans. Faraday Soc. 48 (1952) 658.
[23] G.C. Bond, G. Webb, P.B. Wells, J.M. Winterbottom, J. Catal. 1 (1962) 74.
[24] R.S. Mann, K.C. Khulbe, J. Catal. 13 (1969) 25.
[25] J.J. Phillipson, P.B. Wells, G.R. Wilson, J. Chem. Soc. A (1969) 1351.
[26] P.B. Wells, G.R. Wilson, J. Chem. Soc. (1970) 2442.
[27] Y. Segura, N. López, J. Pérez-Ramírez, J. Catal. 247 (2007) 383.
[28] J.A. Peña, J. Herguido, C. Guimon, A. Monzón, J. Santamaría, J. Catal. 159 (1996) 313.
[29] J.C. Rodríguez, A.J. Marchi, A. Borgna, A. Monzón, J. Catal. 171 (1997) 268.

[30] A. Monzón, E. Romeo, C. Royo, R. Trujillano, F.M. Labajos, V. Rives, Appl. Catal. A 185 (1999) 53.
[31] R.G. Oliver, P.B. Wells, J. Catal. 47 (1977) 364.
[32] Y. Okamoto, K. Fukino, T. Imanaka, S. Teranishi, J. Catal. 74 (1982) 173.
[33] A.F. Benton, P.H. Emmett, J. Am. Chem. Soc. 46 (1924) 2728.
[34] F. Cavani, F. Trifirò, A. Vaccari, Catal. Today 11 (1991) 173.
[35] M. Bellotto, B. Rebours, O. Clause, J. Lynch, J. Phys. Chem. B 100 (1996) 8527.
[36] J. Pérez-Ramírez, G. Mul, F. Kapteijn, J.A. Moulijn, J. Mater. Chem. 11 (2001) 821.
[37] S. Abelló, J. Pérez-Ramírez, Adv. Mater. 18 (2006) 2436.
[38] D. Briggs, M.P. Seah (Eds.), Practical Surface Analysis, vol. 1, Auger and X-Ray Photoelectron Spectroscopy, John Wiley and Sons, Chichester, 1994.
[39] O. Clause, B. Rebours, E. Merlen, F. Trifiró, A. Vaccari, J. Catal. 133 (1992) 231.
[40] L.E. Alzamora, J.H. Ross, E.C. Kruissink, L.L. van Reijen, J. Chem. Soc. Faraday Trans. 77 (1981) 665.
[41] O. Clause, M.G. Coelho, M. Gazzano, D. Matteuzzi, F. Trifirò, A. Vaccari, Appl. Clay Sci. 8 (1993) 169.
[42] D.C. Puxley, I.J. Kitchener, C. Komodromos, N.D. Parkyns, in: G. Poncelet, P. Grange, P.A. Jacobs (Eds.), Preparation of Catalysts III, in: Stud. Surf. Sci. Catal., Elsevier Science, 1983, p. 237.
[43] R.K. Datta, R. Roy, Am. Mineral. 53 (1968) 1456.
[44] J. Pérez-Ramírez, S. Abelló, N.M. van der Pers, J. Phys. Chem. C 111 (2007) 3642.
[45] F.-W. Chang, M.-S. Kuo, M.-T.T.-C. Hsieh, J. Chem. Tech. Biotechnol. 79 (2004) 691.
[46] K.V.R. Chary, P.V.R. Rao, V. Vishwanathan, Catal. Commun. 7 (2006) 974.
[47] P. Arnoldy, J.A. Moulijn, J. Catal. 93 (1985) 38.
[48] D. Tichit, F. Medina, B. Coq, R. Dutartre, Appl. Catal. A 159 (1997) 241.
[49] F. Basile, L. Basini, M.D. Amore, G. Fornasari, A. Guarinoni, D. Matteuzzi, G.D. Piero, F. Trifirò, A. Vaccari, J. Catal. 173 (1998) 247.
[50] L. Zhang, J. Zhu, X. Jiang, D.G. Evans, F. Li, J. Phys. Chem. Solids 67 (2006) 1678.
[51] A.N. Mansour, Surf. Sci. Spectra 3 (1996) 239.
[52] L. Salvati, L.E. Makovsky, J.M. Stencel, F.R. Brown, D.M. Hercules, J. Phys. Chem. 85 (1981) 3700.
[53] B. Rebours, J.-B. d'Espinose de la Caillerie, O. Clause, J. Am. Chem. Soc. 116 (1994) 1707.
[54] F. van Looij, J.W. Geus, J. Catal. 168 (1997) 154.
[55] C. Guimon, A. Auroux, E. Romeo, A. Monzón, Appl. Catal. A 251 (2003) 199.
[56] J. Horiuti, M. Polanyi, Trans. Faraday Soc. 30 (1934) 1164.
[57] J.A. Peña, A. Monzón, J. Santamaría, J. Catal. 142 (1993) 59.
[58] S.D. Jackson, N.J. Casey, J. Chem. Soc. Faraday Trans. 91 (1995) 3269.
[59] N. Sheppard, J.W. Ward, J. Catal. 15 (1969) 50.
[60] J. Wood, M.J. Alldrick, J.M. Winterbottom, E.H. Stitt, S. Bailey, Catal. Today 128 (2007) 52.